Accelerated Publications

Location of the Membrane-Docking Face on the Ca^{2+}-Activated C2 Domain of Cytosolic Phospholipase A_2†

Eric A. Nalefski and Joseph J. Falke*

Department of Chemistry and Biochemistry, University of Colorado, Boulder, Colorado 80309-0215

Received October 2, 1998

ABSTRACT: Docking of C2 domains to target membranes is initiated by the binding of multiple Ca^{2+} ions to a conserved array of residues imbedded within three otherwise variable Ca^{2+}-binding loops. We have located the membrane-docking surface on the Ca^{2+}-activated C2 domain of $cPLA_2$ by engineering a single cysteine substitution at 16 different locations widely distributed across the domain surface, in each case generating a unique attachment site for a fluorescein probe. The environmental sensitivity of the fluorescein-labeled cysteines enabled identification of a localized region that is perturbed by Ca^{2+} binding and membrane docking. Ca^{2+} binding to the domain altered the emission intensity of six fluoresceins in the region containing the Ca^{2+}-binding loops, indicating that Ca^{2+}-triggered environmental changes are localized to this region. Similarly, membrane docking increased the protonation of six fluoresceins within the Ca^{2+}-binding loop region, indicating that these three loops also are directly involved in membrane docking. Furthermore, iodide quenching measurements revealed that membrane docking sequesters three fluorescein labeling positions, Phe^{35}, Asn^{64}, and Tyr^{96}, from collisions with aqueous iodide ion. These sequestered residues are located within the identified membrane-docking region, one in each of the three Ca^{2+}-binding loops. Finally, cysteine substitution alone was sufficient to dramatically reduce membrane affinity only at positions Phe^{35} and Tyr^{96}, highlighting the importance of these two loop residues in membrane docking. Together, the results indicate that the membrane-docking surface of the C2 domain is localized to the same surface that cooperatively binds a pair of Ca^{2+} ions, and that the three Ca^{2+}-binding loops themselves provide most or all of the membrane contacts. These and other results further support a general model for the membrane specificity of the C2 domain in which the variable Ca^{2+}-binding loops provide headgroup recognition at a protein-membrane interface stabilized by multiple Ca^{2+} ions.

The C2 domain is a membrane-targeting module present in numerous eukaryotic proteins that mediate critical cellular processes. Such processes include lipid modification and release of lipid-derived second messengers, protein phosphorylation, regulation of membrane-bound GTPases, vesicular transport, protein ubiquitination, and membrane pore formation (reviewed in refs *1*−*4*). C2 domains are composed of an eight-stranded antiparallel β-sandwich (*5*−*10*) and have been shown to bind to phospholipid membranes in a Ca^{2+}-dependent manner in vitro, although exceptions that bind in a Ca^{2+}-independent manner are known (reviewed in refs *1*−*4*). In many signaling pathways, the C2 domain serves as a Ca^{2+}-regulated on−off switch that recruits specific enzymes to membranes, thereby initiating a myriad of critical regulatory events involving lipids or membrane-bound target proteins.

The regulatory role of the C2 domain is perhaps best understood in the 85 kDa cytosolic phospholipase A_2 ($cPLA_2$),[1] a Ca^{2+}-dependent enzyme that cleaves membrane glycerophospholipids into lysophospholipids and free arachidonic acid, both of which are important mediators of normal and pathological processes (reviewed in refs *11* and *12*). In $cPLA_2$, the C2 domain binds Ca^{2+} and recruits $cPLA_2$ to phospholipid membranes, bringing a Ca^{2+}-independent catalytic domain into contact with its membrane-sequestered substrate (*13*−*15*). Equilibrium and kinetic Ca^{2+}-binding measurements have shown that the $cPLA_2$ C2 domain binds two Ca^{2+} ions with positive cooperativity and that the same stoichiometry is observed when the Ca^{2+}-activated domain docks to membranes (*16*). Recent crystallographic and NMR structural studies have confirmed that the $cPLA_2$ C2 domain binds two Ca^{2+} ions (*9*, *10*), whereas structural studies of other C2 domains have indicated the binding of as many as three Ca^{2+} ions (*8*, *17*, *44*). Such diversity in Ca^{2+} binding is reminiscent of the functional heterogeneity observed for the EF-hand motif, where the stoichiometry, cooperativity,

* Corresponding author. Tel: 303-492-3503. Fax: 303-492-5894. E-mail: falke@colorado.edu.

† Support provided by NIH Grant GM R01-48203 (J.J.F.) and NIH Postdoctoral Fellowship GM-18303 (E.A.N.).

[1] Abbreviations: $cPLA_2$, cytosolic phospholipase A_2; PC, phosphatidylcholine; PIPES, piperazine-*N*,*N*′-bis(2-ethanesulfonic acid); EDTA, ethylenediaminetetraacetic acid; IAF, 5-iodoacetamidofluorescein; FRET, fluorescence resonance energy transfer; PC, 1-palmitoyl-2-oleoyl-*sn*-

10.1021/bi982372e CCC: $15.00
Published on Web 12/03/1998

and affinity of Ca^{2+}-binding vary widely for EF-hand domains from different signaling pathways (*18*, *19*).

The exact mechanism by which C2 domains bind to phospholipid membranes in response to Ca^{2+} is currently unknown. Two extreme models for membrane docking induced by Ca^{2+} binding to C2 domains include the "allosteric" and "Ca^{2+}-bridging" models. Ca^{2+} binding to one site in the domain may induce allosteric changes elsewhere to create a phospholipid-binding interface, a mechanism analogous to the "Ca^{2+}-myristoyl switch" employed by the EF-hand protein recoverin (*20*). Alternatively, Ca^{2+} could act as a bridge between the domain and the phospholipid surface, simultaneously coordinated by the domain and the phospholipid headgroup, a mechanism utilized by the annexin class of Ca^{2+}-dependent membrane-binding proteins (*21*). Several recent findings support a model in which the Ca^{2+}-binding site lies near the membrane in the complex (*6*−*10*, *17*, *22*−*25*), including the observation that Ca^{2+} ions become occluded upon membrane docking (*16*). However, to rigorously map the outlines of the membrane-docking site, it is necessary to examine all regions of the C2 domain surface for Ca^{2+}-induced membrane interactions. If the Ca^{2+}-binding cleft plays a dominant role in membrane docking, then protein−membrane interactions should be detected for Ca^{2+}-binding loops but not for other regions.

The goal of the present study has been to determine the outline of the membrane-docking face. The approach utilized 16 engineered cysteines that were individually substituted for solvent-exposed residues spanning all surface regions of the $cPLA_2$ C2 domain. The effect of these substitutions on Ca^{2+} binding and membrane docking were, with a few interesting exceptions, relatively nonperturbing. The cysteines were covalently derivatized with a thiol-selective fluorescein label to place a single fluorophore at a series of specific surface locations. The effects of Ca^{2+} binding and membrane docking on spectral properties of the site-specific fluoresceins were assessed to monitor environmental changes at these locations during binding events. Membrane-induced protection of the fluorescein probes from iodide quenching was also measured to identify positions that are buried in the protein−membrane interface. The results indicate that all three of the Ca^{2+}-binding loops of the C2 domain are involved in direct protein−membrane contacts, whereas other regions of the protein surface are more distal to the membrane.

MATERIALS AND METHODS

Protein Production. Two methods were used to generate cysteine variants. In the first, plasmid pTrc-$cPLA_2$(1−138), encoding the first 138 residues of human $cPLA_2$ (*15*), was altered via the Unique Site Elimination protocol (Pharmacia). Antisense mutagenic oligonucleotides contained the codon for cysteine and silent mutations to create or eliminate restriction enzyme sites (*26*). Mutant plasmids were identified by restriction enzyme digestion. The other method, which was more efficient for the majority of variants, utilized phagemid mutagenesis. The 1.2 kb *Eco*RI−*Sca*I fragment from the vector pRSET A (Invitrogen), encoding the M13 origin of replication, was substituted for the 0.8 kb *Eco*RI−*Sca*I fragment of pTrc-$cPLA_2$(1−138). The resulting plasmid, f1-pTrc-$cPLA_2$(1−138), was used to generate a uracil-labeled single-stranded DNA template for site-directed mutagenesis as described (*26*).

Wild-type and variant C2 domains were expressed in *E. coli*, refolded from inclusion bodies, and affinity-purified to homogeneity on a phosphatidylcholine (PC) matrix as described (*16*). Monomers were isolated by passing purified material over a Sephadex G-75 column run in standard assay buffer [100 mM KCl and 20 mM piperazine-*N*,*N*′-bis(2-ethanesulfonic acid) (PIPES), pH 7.0, with KOH] containing 1 mM $CaCl_2$. Proteins were stored in assay buffer containing 100 μM dithiothreitol and 100 μM ethylenediaminetetraacetic acid (EDTA) to prevent metal-catalyzed disulfide formation. Protein concentration was determined spectroscopically as described (*16*). Proteins (∼50 μM) were labeled with 300 μM 5-iodoacetamidofluorescein (IAF, Molecular Probes) for 1 h at room temperature in the dark. Once labeled, proteins were kept in the dark to prevent photobleaching of the attached fluorophore. Free probe was removed by passing proteins twice over Sephadex G-10 spin columns equilibrated in assay buffer (*27*). Removal of free probe was confirmed by sodium dodecyl sulfate−polyacrylamide gel electrophoresis. Labeled proteins were snap frozen, stored in liquid nitrogen at −70 °C, and rapidly thawed prior to use.

Ligand-Binding Assays. Fluorescence spectroscopy was carried out on an SLM 48000S fluorescence spectrometer at 25 °C. For assays involving unlabeled proteins, intrinsic Trp^{71} emission from the domain was monitored throughout at a fixed wavelength (λ_{ex} = 284 nm, λ_{em} = 325 nm) or by recording emission spectra (λ_{ex} = 284 nm, λ_{em} = 300−400 nm). Ca^{2+}-induced increases in Trp^{71} emission revealed Ca^{2+} binding (*16*). Membrane docking was measured by monitoring quenching of Trp^{71} emission due to fluorescence resonance energy transfer (FRET) to sonicated vesicles composed of 97.5% (mol/mol) PC (1-palmitoyl-2-oleoyl-*sn*-glycero-3-phosphocholine, Avanti Polar Lipids) and 2.5% (mol/mol) of the acceptor dansyl-PE [*N*-(5-dimethylaminonaphthalene-1-sulfonyl)-1,2-dihexadecanoyl-*sn*-glycero-3-phosphoethanolamine, Molecular Probes] (*16*). Ca^{2+} binding was initiated by adding 2 mM $CaCl_2$ to protein (∼0.5 μM) incubated in assay buffer containing 1 mM EDTA. Membrane docking by Ca^{2+}-loaded protein was then recorded by adding a concentrated stock of vesicles. The FRET-induced decrease in Trp^{71} emission (ΔF) was best-fit to the equation for a homogeneous population of single independent sites:

$$\Delta F = \Delta F_{max}\left(\frac{[PC]}{K_D^{PC} + [PC]}\right) \quad (1)$$

where K_D^{PC} represents the apparent dissociation constant of Ca^{2+}-loaded protein for PC membranes, ΔF_{max} represents the calculated maximal fluorescence change, and [PC] represents the total PC concentration in the sonicated vesicle suspension. This assay yielded average K_D^{PC} values of 15 ± 4 μM for the wild-type C2 domain (n = 3). Equivalent results were obtained when FRET was monitored by dansyl-PE emission rather than donor Trp^{71} quenching (*16*).

glycero-3-phosphocholine; dansyl-PE, *N*-(5-dimethylaminonaphthalene-1-sulfonyl)-1,2-dihexadecanoyl-*sn*-glycero-3-phosphoethanolamine; Texas Red-PE, *N*-(Texas Red sulfonyl)-1,2-dihexadecanoyl-*sn*-glycero-3-phosphoethanolamine; SytI, synaptotagmin, I; PKCβ, protein kinase Cβ.

Table 1: Properties of Cysteine-Substituted Variants of the cPLA$_2$ C2 Domain

	K_D^{PC} (μM)		(−) vesicles			(+) vesicles		
variant	unlabeled C2[a]	labeled C2[b]	K_{SV} (M^{-1})[c]	τ_0 (ns)[d]	$k_q \times 10^{-9}$ (s^{-1} M^{-1})[e]	K_{SV} (M^{-1})[c]	τ_0 (ns)[d]	$k_q \times 10^{-9}$ (s^{-1} M^{-1})[e]
T21C	12 ± 1	25 ± 7	6.8 ± 0.1	3.8 ± 0.2	1.8 ± 0.1	5.8 ± 0.1	3.8 ± 0.2	1.5 ± 0.1
F35C	60 ± 20	36 ± 6	8.8 ± 0.1	3.2 ± 0.1	2.8 ± 0.1	2.6 ± 0.1	3.4 ± 0.1	0.8 ± 0.1
L39C	23 ± 6	46 ± 2	5.4 ± 0.1	2.8 ± 0.1	1.9 ± 0.1	5.5 ± 0.1	3.3 ± 0.1	1.7 ± 0.1
S51C	18 ± 7	8 ± 2	4.9 ± 0.1	3.1 ± 0.1	1.6 ± 0.1	5.3 ± 0.1	3.1 ± 0.1	1.7 ± 0.1
R59C	11 ± 3	18 ± 5	6.7 ± 0.1	3.5 ± 0.2	1.9 ± 0.1	6.2 ± 0.1	3.4 ± 0.2	1.8 ± 0.1
N64C	23 ± 6	12 ± 2	6.7 ± 0.1	2.4 ± 0.1	2.8 ± 0.2	5.2 ± 0.1	3.2 ± 0.1	1.6 ± 0.1
N68C	13 ± 3	8.5 ± 0.8	6.0 ± 0.2	3.5 ± 0.1	1.7 ± 0.1	5.9 ± 0.1	3.6 ± 0.1	1.6 ± 0.1
N72C	9 ± 4	15 ± 7	9.8 ± 0.1	3.5 ± 0.2	2.8 ± 0.2	7.6 ± 0.1	3.4 ± 0.1	2.2 ± 0.1
I78C	8 ± 2	8 ± 1	5.2 ± 0.1	3.1 ± 0.1	1.7 ± 0.1	6.1 ± 0.1	3.0 ± 0.1	2.0 ± 0.1
N82C	11 ± 4	12 ± 4	6.3 ± 0.1	2.9 ± 0.1	2.2 ± 0.1	5.4 ± 0.1	2.8 ± 0.1	1.9 ± 0.1
Y96C	80 ± 20	90 ± 20	9.9 ± 0.2	3.2 ± 0.1	3.1 ± 0.2	2.2 ± 0.1	3.2 ± 0.1	0.7 ± 0.1
M98C	14 ± 2	3.0 ± 0.3	6.9 ± 0.1	3.6 ± 0.1	1.9 ± 0.1	5.9 ± 0.1	3.8 ± 0.1	1.6 ± 0.1
T106C	22 ± 8	31 ± 6	4.1 ± 0.1	3.5 ± 0.1	1.2 ± 0.1	3.9 ± 0.1	3.7 ± 0.1	1.0 ± 0.1
K113C	17 ± 5	14 ± 2	5.2 ± 0.1	3.7 ± 0.1	1.4 ± 0.1	4.8 ± 0.1	3.7 ± 0.1	1.3 ± 0.1
N125C	12 ± 2	15 ± 1	5.7 ± 0.1	4.0 ± 0.1	1.4 ± 0.1	5.8 ± 0.1	3.8 ± 0.1	1.5 ± 0.1
E129C	10 ± 1	11 ± 1	4.8 ± 0.1	3.6 ± 0.1	1.3 ± 0.1	5.2 ± 0.1	3.7 ± 0.2	1.4 ± 0.1

[a] Apparent equilibrium dissociation constant (average ± SEM, $n = 3$ independent determinations) for PC binding measured in FRET titrations of Ca^{2+}-loaded C2 domains with acceptor membranes as in Figure 1A. A value of 15 ± 4 μM was measured for the wild-type domain ($n = 3$). [b] Apparent equilibrium dissociation constant (average ± SEM, $n = 3$) for PC binding measured in FRET titrations of Ca^{2+}-loaded IAF-labeled C2 domain with acceptor membranes as in Figure 1B. [c] Iodide quenching constant determined in the absence or presence of PC vesicles as in Figure 3, panels A and B. Errors represent uncertainties in best-fit determination. [d] Fluorescein fluorescence lifetime (average ± SEM) determined by phase modulation method. [e] Bimolecular quenching rate constant for iodide quenching of fluorescein fluorescence determined as described in text. Uncertainties represent errors propagated from K_{SV} and τ_0.

To measure membrane docking by IAF-labeled proteins, the fluorescein emission of labeled protein (~0.5 μM) in assay buffer containing 2 mM $CaCl_2$ and 1 mM EDTA was monitored ($\lambda_{ex} = 492$ nm, $\lambda_{em} = 519$ nm) following addition of vesicles containing a FRET acceptor. These vesicles were composed of 97.5% (mol/mol) PC and 2.5% (mol/mol) of the acceptor Texas Red-PE [*N*-(Texas Red sulfonyl)-1,2-dihexadecanoyl-*sn*-glycero-3-phosphoethanolamine, Molecular Probes]. K_D^{PC} was determined by best-fitting the normalized fluorescein emission change to eq 1. For all ligand-triggered fluorescence and FRET changes, reversibility of binding was confirmed by addition of excess EDTA at the end of the titration.

Measuring Effects of Ligand Binding on Fluorescein Emission. To measure effects of Ca^{2+} and PC membranes on IAF-labeled domains, the change in fluorescein emission of labeled protein (~0.5 μM) incubated in assay buffer containing 1 mM EDTA was monitored upon successive addition of 2 mM $CaCl_2$ and vesicles (250 μM PC), respectively. Fluorescein emission was monitored either at a single emission wavelength ($\lambda_{ex} = 492$ nm, $\lambda_{em} = 519$ nm) or by recording emission spectra ($\lambda_{ex} = 492$ nm, $\lambda_{em} = 500-550$ nm). Fluorescence changes due to Ca^{2+} were normalized to the fluorescence intensity of protein in buffer plus EDTA. Fluorescence changes due to PC were normalized to the fluorescein emission of protein loaded with Ca^{2+}. Emission spectra were normalized to the maximal emission intensity of protein in assay buffer plus EDTA. Other experiments monitored fluorescein mono- and dianions by collecting excitation spectra ($\lambda_{ex} = 400-525$ nm, $\lambda_{em} = 600$ nm) and emission spectra ($\lambda_{ex} = 437$ nm, $\lambda_{em} = 475-600$ nm) of IAF-labeled protein in assay buffer plus 1 mM EDTA upon successive additions of 2 mM $CaCl_2$, vesicles (250 μM PC), and excess EDTA.

Iodide Quenching. Iodide quenching was carried out by preparing solutions of IAF-labeled proteins (~0.5 μM), with or without vesicles (250 μM PC), in buffer containing 20 mM PIPES, pH 7.0, 2 mM $CaCl_2$, 1 mM EDTA, and either 200 mM KCl or KI. The KI was diluted from a 2 M stock prepared with 0.5 mM $Na_2S_2O_3$ to prevent I_2 formation (*28*). Aliquots of samples in KCl were removed and replaced with aliquots from samples in KI to incrementally increase KI concentration and to maintain [KI] + [KCl] = 200 mM. Relative quenching was calculated as the ratio F_0/F, where F and F_0 represent the fluorescein emission ($\lambda_{ex} = 492$ nm, $\lambda_{em} = 519$ nm) with and without added iodide, respectively. Relative quenching was best-fit to the Stern−Volmer equation:

$$F_0/F = K_{SV}[KI] + 1 \quad (2)$$

where K_{SV} represents the Stern−Volmer quenching constant (*29*).

The lifetime of each fluorescein label was determined using the phase-modulation method (*30*). Briefly, exciting light ($\lambda_{ex} = 488$ nm) was generated by a 6 W Coherent Innova argon ion laser. The intensity of this light was sinusoidally modulated at 33 MHz by the Pockel cell of an SLM 48000S phase modulation spectrometer, and the fluorescence lifetime (τ_0) was calculated from the phase shift between the exciting light and the light emitted by the sample ($\lambda_{em} = 550$ nm). Recorded values represent averages (±SEM) of 6−10 determinations. A scattering glycogen sample provided a zero-phase shift control. Samples consisted of IAF-labeled proteins (~0.5 μM), with or without vesicles (250 μM PC), in assay buffer containing 2 mM $CaCl_2$ and 1 mM EDTA. The resulting lifetimes, together with the Stern−Volmer constant K_{SV} enabled calculation of the bimolecular quenching rate constant for iodide (see below).

RESULTS

Effects of Cysteine Substitutions on Protein Folding and Membrane Docking. Single cysteines were individually substituted for 16 surface residues in the cPLA$_2$ C2 domain

(Table 1), which contains no intrinsic cysteines. Positions for substitution were chosen such that the β-carbon of the side chain is highly solvent exposed in the crystal structure of the $cPLA_2$ C2 domain, yielding minimal structural perturbation and maximal surface localization for fluorophores attached to the engineered sulfhydryl. In addition, these positions were chosen to sample all regions of the C2 domain surface. Cysteine-substituted variants were isolated as inclusion bodies, refolded in vitro, and then purified to homogeneity by Ca^{2+}-driven adsorption to a phospholipid matrix followed by size-exclusion chromatography. Variants F35C and Y96C yielded poor recovery in the affinity column step and were thus purified by a different procedure involving size-exclusion chromatography alone.

The effect of the cysteine substitutions on the intrinsic tryptophan fluorescence of the apo-domain was determined to test for perturbations. All variant C2 domains displayed an intrinsic fluorescence maximum near 325 nm (for $\lambda_{ex} =$ 284 nm), characteristic of the sole tryptophan, Trp^{71}, of the wild-type C2 domain (*16*). This tryptophan is highly conserved among C2 domains (*1*−*3*) and is buried in the protein core. The fact that the native emission maximum is not shifted indicates that the substituted cysteines do not cause global unfolding or dramatic perturbations in the environment of Trp^{71}. Addition of saturating concentrations of Ca^{2+} to all variant C2 domains resulted in at least 17% enhancement of the intrinsic tryptophan emission (data not shown). This fluorescence increase, also observed in the wild-type C2 domain, is due to an environmental perturbation stemming from a combination of conformational, electrostatic, and dynamic changes transmitted from the Ca^{2+}-binding sites to Trp^{71} (*16*). It follows that the variant domains retain the ability to bind Ca^{2+} and transmit information to the buried indole. Interestingly, five variants yielded larger-than-native enhancements of Trp^{71} fluorescence upon Ca^{2+} binding: T21C (33 ± 3% increase compared to 18 ± 1% for the wild-type domain), R59C (33 ± 1%), N68C (121 ± 1%), N72C (77 ± 1%), and E129C (28 ± 1%) ($n = 3$ experiments). These substitutions lie in the vicinity of Trp^{71} and alter its fluorescence quantum yield in either the apo- or Ca^{2+}-occupied state; however, they do not significantly affect the affinity of the Ca^{2+}-bound C2 domain for PC membranes (see below).

Membrane docking by wild-type and variant C2 domains was also compared to test for perturbations due to the cysteine substitutions. Ca^{2+}-induced binding of the $cPLA_2$ C2 domain to PC membranes enhances the intrinsic Trp^{71} emission, indicating that membrane-docking further alters the environment of the buried indole ring (*16*). When the PC membranes contain a small quantity of dansyl-PE (2.5% mol/mol), the Trp^{71} emission of the membrane-bound domain is quenched by FRET to the dansyl acceptor probe (*16*). This FRET assay for membrane docking was used to quantify the lipid concentration needed to drive the protein−membrane association (Figure 1A), yielding an apparent equilibrium dissociation constant for the binding of the Ca^{2+}-saturated C2 domain to PC vesicles (K_D^{PC}, Table 1). The wild-type C2 domain bound with an average apparent K_D^{PC} of 15 μM. Fourteen of the 16 variant C2 domains bound with comparable affinities, K_D^{PC} ranging 8−23 μM. However, variants F35C (Figure 1A) and Y96C exhibited

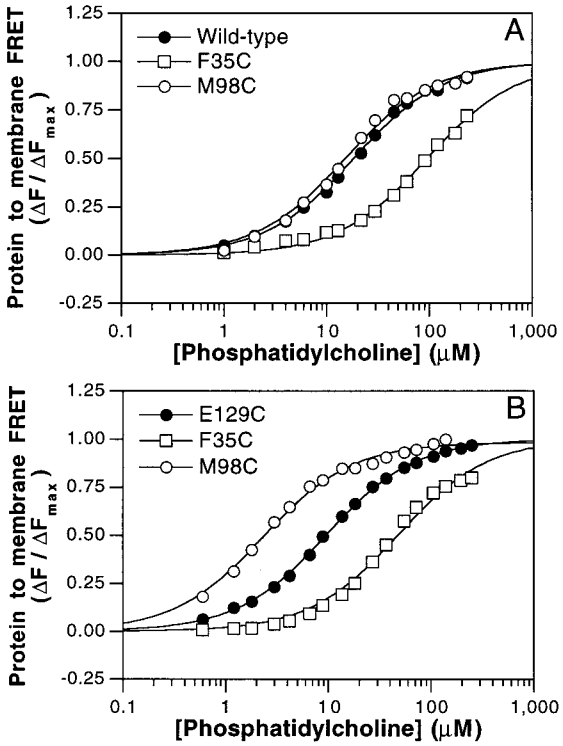

FIGURE 1: Docking of unlabeled and labeled C2 domain variants to PC membranes. (A) Ca^{2+}-induced docking of unlabeled wild-type (closed circles) and representative variant C2 domains (open symbols) to PC vesicles spiked with dansyl-PE (2.5% mol/mol), detected as protein-to-membrane FRET. Normalized quenching ($\Delta F/F_{max}$) of the intrinsic Trp^{71} donor by increasing concentrations of the acceptor membrane was best-fit by eq 1 (see text), yielding the solid curves and binding parameters summarized in Table 1. (B) Ca^{2+}-induced docking of representative IAF-labeled variants to PC vesicles spiked with Texas Red-PE (2.5% mol/mol) was detected by measuring labeled protein-to-membrane FRET. Data were analyzed as in panel A. Experimental conditions in both panels A and B: 100 mM KCl, 20 mM PIPES, pH 7.0, 2 mM $CaCl_2$, 1 mM EDTA; ~0.5 μM C2 domain; 25 °C.

significantly lower affinities, yielding K_D^{PC} values of 60 and 80 μM, respectively. These results, which explain the failure of these variants to bind efficiently to the PC affinity matrix during purification, indicate that substitution of cysteine for Phe^{35} and Tyr^{96} significantly interferes with Ca^{2+}-induced phospholipid docking. In contrast, cysteine substitutions elsewhere in the C2 domain are less perturbing. Overall, the cysteine substitutions have little effect on Ca^{2+} binding and, with the exception of F35C and Y96C, membrane docking.

Effect of Probe Attachment on Membrane Docking. The introduced cysteines were selectively labeled with the fluorescent thiol-alkylating reagent 5-iodoacetamidofluorescein (IAF). Membrane docking by each labeled, Ca^{2+}-loaded domain was detected as quenching of its fluorescein emission by PC vesicles containing a small quantity of Texas Red-PE (2.5% mol/mol) as a FRET acceptor (Figure 1B, Table 1). To varying degrees, this observed fluorescein quenching involves both FRET to the Texas Red acceptor and additional quenching observed upon docking to membranes lacking the acceptor (see below). Fifteen labeled C2 domains bound PC membranes with affinities comparable to their unlabeled counterparts (Table 1), including those C2 domains that bind with wild-type affinity and variants F35C (Figure 1B) and Y96C, both of which retained their sub-wild-type affinity when labeled. However, labeling of the M98C variant caused

a modest increase in membrane affinity: the K_D^{PC} of 14 μM for the unlabeled protein was lowered to 3 μM for the labeled protein, suggesting that placement of fluorescein at this position stabilizes membrane docking (Figure 1, Table 1). It is likely that this position lies at or near the membrane-docking surface (see Discussion).

Use of Fluorescein as an Environmental Probe for Ca^{2+} Binding and Membrane Docking. Fluorescein has been used as a probe to monitor local environmental conditions including pH (*31*), surface potential (*32*), and dielectric constant (*33*) in biological systems. For each IAF-labeled variant, the effect of saturating Ca^{2+} and PC concentrations on the fluorescein emission spectrum was determined. The results reveal that each ligand triggers environmental changes localized to specific regions of the domain. Representative spectra are illustrated in Figure 2, panels A and B. Changes in fluorescein emission intensity at the emission maximum of 519 nm (for $\lambda_{ex} = 492$ nm) were measured and normalized to the initial intensity in the absence of ligand (Figure 2, panels C and D).

Ca^{2+} addition triggered a minimal decrease (<10%) of the fluorescein emission at 10 of the 16 labeling positions, as illustrated by labeled I78C (Figure 2, panels A and C). In contrast, Ca^{2+} addition significantly increased the emission of the labeled Y96C variant by ~17% (Figure 2, panels B and C) and also increased the emission of the labeled F35C, N68C and E129C variants (Figure 2C). In contrast, Ca^{2+} addition dramatically decreased the emission of the labeled L39C and N64C variants (Figure 2C). These results indicate that the six side-chain positions 35, 39, 64, 68, 96, and 129 are sensitive to local environmental changes that accompany Ca^{2+} binding. Five of these residues are found in Ca^{2+}-binding loops (35, 39, 64, 68, and 96) whereas position 129 lies in a β-strand position proximal to the loops (see Discussion). The first Ca^{2+}-binding loop contains a short helical region that includes residues 35 and 39.

Membrane docking also triggered changes in fluorescein emission at certain labeling positions. The representative IAF-labeled variant I78C and nine other labeled variants yielded minimal change in fluorescein emission (<10%) upon addition of pure PC membranes (Figure 2, panels A and D). However, addition of PC vesicles did trigger a ~70% fluorescein emission decrease in the labeled variant Y96C and significantly decreased the emission of labeled variants F35C, L39C, N64C, M98C, and E129C to differing extents (Figure 2, panels B and D). For representative labeled variants I78C and Y96C (Figure 2, panels A and B) and all other variants (data not shown), addition of excess EDTA returned fluorescein emission to within 10% of the starting emission recorded in the absence of added Ca^{2+} and PC, indicating that the fluorescence changes are reversible. Thus, the six side chain positions 35, 39, 64, 96, 98, and 129 are sensitive to local environmental changes accompanying Ca^{2+}-induced membrane docking. Five of these positions are located in Ca^{2+}-binding loops (35, 39, 64, 96, and 98) whereas position 129 lies in a β-strand region proximal to the loops (see Discussion).

Multiple protonation species of fluorescein exist in solution, including neutral, monoanionic, and dianionic species that differ in fluorescence quantum yield and optimal wavelengths for absorbance and fluorescence emission (*34*). The pH and dielectric sensitivity of fluorescein emission stems largely from the equilibrium between the dominant dianion and the less fluorescent monoanion (pK_a ~6.3) (*33*, *34*). These species have different excitation and emission wavelengths (*34*), enabling detection of equilibrium shifts between their respective protonation states. Excitation and emission spectra were collected for IAF-labeled variants that underwent fluorescein emission changes induced by saturating concentrations of Ca^{2+} or PC membranes (F35C, L39C, N64C, N68C, Y96C, M98C, and E129C), as well as the control variant I78C, which is unaffected by Ca^{2+} or PC binding. The initial screen used parameters that maximize detection of the fluorescein monoanion ($\lambda_{ex} = 437$ nm, $\lambda_{em} = 600$ nm). Addition of saturating Ca^{2+} alone to each of the selected C2 domains failed to drive detectable interconversion between the fluorescein dianion and monoanion (data not shown). Similarly, addition of saturating Ca^{2+} and PC vesicles to the control-labeled variant I78C failed to drive the interconversion (Figure 2E). However, addition of Ca^{2+} and PC vesicles to labeled Y96C resulted in partial loss of the fluorescein dianion coupled to an increase in the fluorescein monoanion, as indicated by changes at their excitation maxima (~490 nm, shoulder at ~460 nm) and emission maxima (~520 nm, shoulder at ~560 nm), respectively (Figure 2F). Similar membrane-induced loss of dianion and concomitant appearance of monoanion were observed for fluoresceins coupled to variants F35C, L39C, N64C, M98C, and E129C (data not shown). Addition of excess EDTA resulted in conversion back to fluorescein dianion for these six labeled C2 domains (data not shown), demonstrating the reversibility of the interconversion upon disruption of the C2 domain−membrane complex. Together, these results indicate that the pK_a of fluoresceins attached to positions 35, 39, 64, 96, 98, and 129 are raised upon Ca^{2+}-induced membrane docking as a consequence of localized environmental changes, most likely due to membrane proximity.

Protection of Site-specific Probes against Iodide Quenching. Collisional encounters between a fluorophore and charged quenchers such as iodide, which are relatively impermeable to proteins and phospholipid membranes, have been used to determine the surface accessibility of fluorophores in proteins and localization of fluorophores in model membranes (*35*, *36*). Since iodide efficiently quenches fluorescein emission (*37*), membrane-docking residues of the C2 domain were identified by the ability of PC membranes to protect against iodide quenching as assessed by Stern−Volmer analysis. Stern−Volmer plots were generated for all Ca^{2+}-loaded, IAF-labeled C2 domains both in the absence and presence of PC membranes, as illustrated for K113C and F35C in Figure 3, panels A and B. All plots were linear with respect to iodide concentration, as expected for a homogeneous population of fluorophores. The resulting slopes provide the Stern−Volmer quenching constant K_{SV}, as summarized in Table 1.

The Stern−Volmer constant K_{SV} can be converted to a bimolecular quenching rate constant (k_q), assuming that the fluorescence lifetime (τ_0) in the absence of quencher is known ($k_q = K_{SV}/\tau_0$). The resulting quenching rate constant is directly proportional to the collisional encounters between the fluorophore and the quencher and for charged quenchers such as iodide may be influenced by both electrostatic and steric factors. To determine k_q, the fluorescein emission

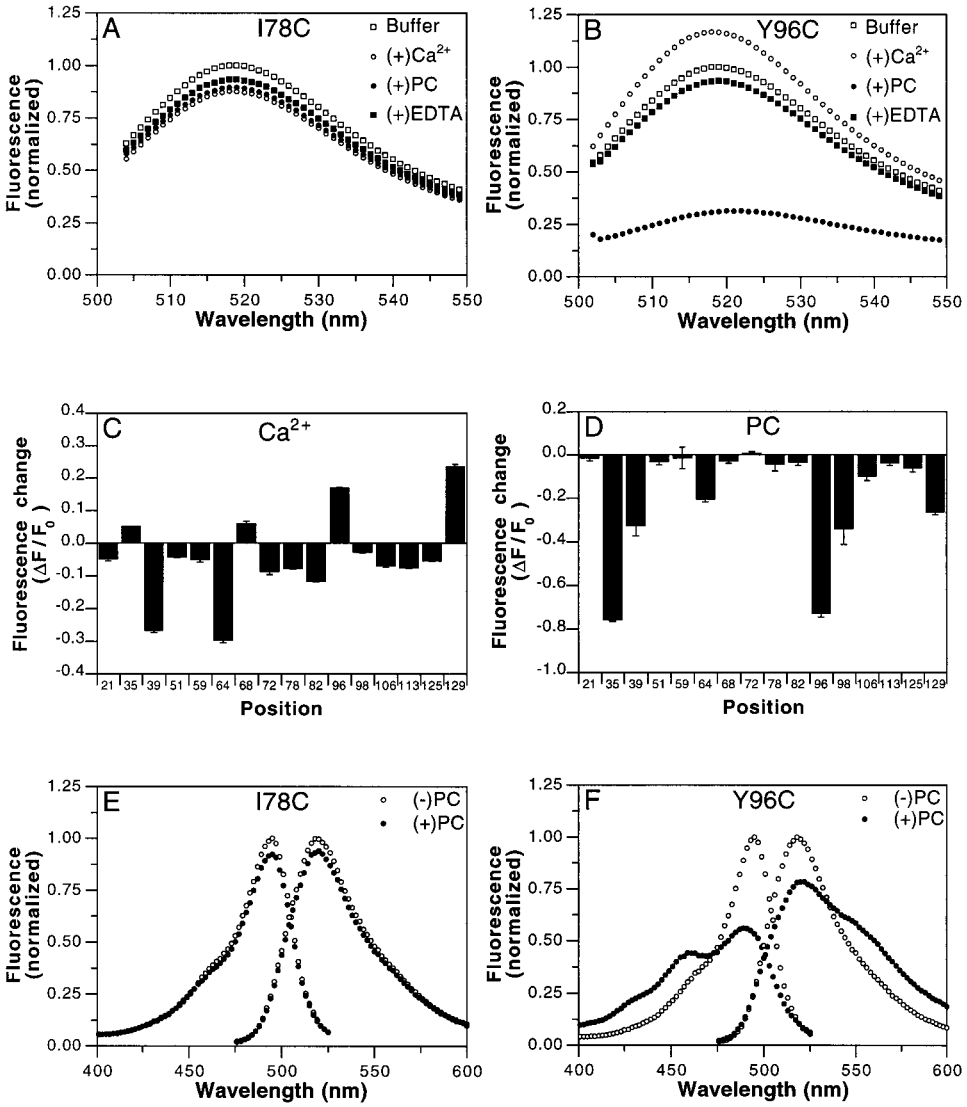

FIGURE 2: Fluorescein emission changes induced by Ca^{2+} binding and membrane docking to labeled C2 domains. (A, B) Fluorescein emission spectra of IAF-labeled variants I78C (A) and Y96C (B) in assay buffer containing 1 mM EDTA (open squares) were recorded upon successive addition of 2 mM $CaCl_2$ (open circles), then vesicles (250 μM PC, closed circles), and finally excess EDTA (closed squares). Spectra were normalized to the maximal fluorescence in the initial spectrum. $\lambda_{ex} = 492$ nm. (C) Fluorescein emission changes (ΔF) induced by addition of 2 mM $CaCl_2$ to the IAF-labeled variants in 1 mM EDTA, measured as in panels A and B for several independent experiments ($n = 4-6$) and normalized to the initial fluorescence prior to Ca^{2+} addition (F_0). Bars indicate average (±SEM). $\lambda_{em} = 519$ nm. (D) Fluorescein emission changes (ΔF) induced by the addition of 250 μM PC vesicles to the IAF-labeled variants in 1 mM EDTA and 2 mM $CaCl_2$, measured as in panels A and B in three independent experiments and normalized to the initial fluorescence prior to vesicle addition (F_0). Bars indicate average (±SEM). $\lambda_{em} = 519$ nm. (E, F) Excitation and emission spectra of fluorescein attached to variants I78C and Y96C in assay buffer containing 1 mM EDTA and 2 mM $CaCl_2$ were recorded in the absence (open circles) or presence of vesicles (250 μM PC, closed circles). Spectra were normalized to the maximal fluorescence prior to vesicle addition. For excitation scan, $\lambda_{em} = 600$ nm; for emission scan, $\lambda_{ex} = 437$ nm. The presence of fluorescein monoanion is indicated by an excitation shoulder at ~460 nm and an emission shoulder at ~560 nm (see Y96C in panel F following addition of PC). Experimental conditions in panels A to F were 100 mM KCl and 20 mM PIPES, pH 7.0; ~0.5 μM C2 domain; 25 °C.

lifetime was measured for each Ca^{2+}-loaded labeled C2 domain in both the absence and the presence of membranes (Table 1). Subsequently, a protection index was calculated for each variant as the ratio of the bimolecular quenching rate constant in the absence of PC membranes to that in the presence of membranes and compared in Figure 3C. For 13 of the 16 labeled C2 domains, protection indices were ~1, demonstrating that membrane binding provided no protection from iodide collisions in the majority of C2 variants. However, the labeled F35C, N64C, and Y96C variants each demonstrated significantly elevated protection indices of 3.6 ± 0.4, 1.7 ± 0.2, and 4.5 ± 0.6, respectively. These results indicate that upon membrane docking, fluoresceins attached to positions 35, 64, and 96 are significantly less accessible to collisions with iodide. Notably, all three of these positions are located on Ca^{2+}-binding loops.

DISCUSSION

Results of this study are summarized in Figure 4, in which the positions of the cysteine substitutions are mapped onto the structure of the $cPLA_2$ C2 domain. Figure 4A summarizes the fluorescein-labeled cysteine positions that are sensitive to Ca^{2+}-triggered environmental changes. Five of these six positions are found in the three Ca^{2+}-binding loops (35, 39, 64, 68, and 96) whereas the other position (129) lies in a β-strand region proximal to the loops. The effect of Ca^{2+}

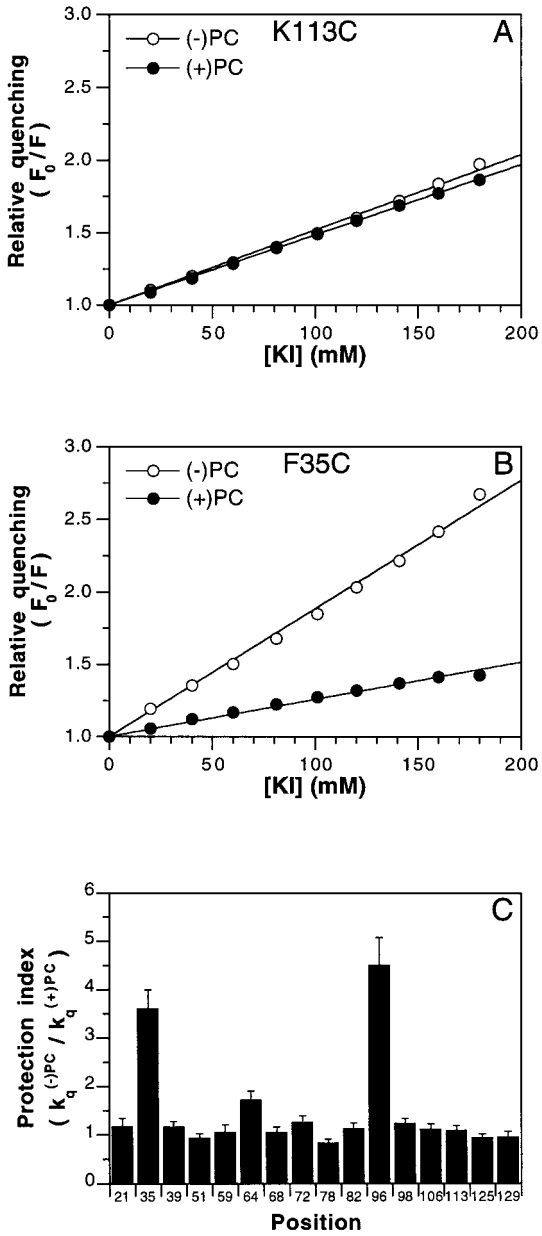

FIGURE 3: Effect of membrane docking on iodide quenching. (A, B) Relative iodide quenching of IAF-labeled K113C and F35C in excess Ca^{2+} with (filled circles) or without (open circles) 250 μM PC vesicles. Relative quenching was calculated as the ratio of fluorescein emission (λ_{ex} = 492 nm, λ_{em} = 519 nm) in the absence of quencher (F_0) to the emission in the presence of the indicated concentration of iodide (F). Solid lines represent best-fit to the Stern−Volmer equation (see text). Results are summarized in Table 1. Experimental conditions: 20 mM PIPES pH 7.0, 2 mM $CaCl_2$, 1 mM EDTA; [KCl] + [KI] maintained at 200 mM. (C) Protection indices were calculated as the ratio of bimolecular quenching rate constant in the absence of membranes to that in the presence of membranes (see Table 1). The indicated error bars are propagated from the Stern−Volmer and lifetime uncertainties.

binding on fluorescein quantum yield at these positions is likely to arise from a combination of structural, electrostatic and dynamic changes in the Ca^{2+}-binding cleft itself, which is formed by the three loops. Electrostatic changes are not large enough to significantly shift the fluorescein pK_a, since there is little effect of Ca^{2+} binding on the protonation level of the fluoresceins. Outside the Ca^{2+}-binding loops, nine of the 10 positions surveyed are insensitive to Ca^{2+} binding. Thus, the environmental changes detected by fluorescein probes are localized to the Ca^{2+}-binding loops and proximal regions of adjoining β-strands. A similar localization was observed in NMR studies of Ca^{2+}-induced chemical shift changes in the $cPLA_2$ and synaptotagmin C2 domains (*10*, *38*).

Membrane-docking causes environmental perturbations at the six fluorescein labeling positions highlighted in Figure 4B. Five of the six positions are found in Ca^{2+}-binding loops (35, 39, 64, 96, and 98) whereas the remaining position (129) lies in a β-strand region proximal to the loops. The membrane-induced changes in fluorescein emission are mechanistically different from the changes induced by Ca^{2+} binding, since at all six sites membrane docking is found to shift the fluorescein protonation state from the predominant dianion to the less fluorescent monoanion. It follows that the pK_a of fluorescein attached at these positions is significantly increased upon membrane docking, most likely due to proximity to the anionic phosphate layer or the low-dielectric region of the bilayer. The other 10 positions surveyed, which lie outside the Ca^{2+}-binding region, are insensitive to membrane docking and thus are more likely to be distant from the membrane surface. On the basis of the strong clustering of fluorescein-labeling positions that detect membrane-induced perturbations, we propose that the three Ca^{2+}-binding loops all directly contact the membrane surface (Figure 4B).

Further support for the involvement of the Ca^{2+}-binding loops in membrane docking is provided by the location of fluorescein-labeling positions that are protected from iodide quenching (Figure 4B). Only the fluoresceins attached to positions 35, 64, and 96 in the three Ca^{2+}-binding loops are protected from collisional encounters with iodide when the C2 domain is docked to target PC membranes. The simplest explanation is that these residues are largely buried within the domain−membrane interface, whereas the remaining labeled residues are largely solvent exposed in both the free and membrane-bound states. The protected positions 35, 64, and 96 are among the six positions that undergo membrane-induced changes in fluorescein emission, confirming that fluorescence changes at these three positions are due to direct membrane contact. Fluoresceins at the three other membrane-perturbed positions (39, 98, and 129) are not protected from iodide quenching, indicating that their membrane-induced fluorescence changes are due to partial burial at the membrane interface or local environmental changes induced by allosteric coupling to the docking site. Allosteric coupling is especially plausible for position 129, which is distal from the Ca^{2+}-binding pocket but contacts the N-terminus of the first Ca^{2+}-binding loop.

The proposed orientation of the membrane-bound domain is also supported by observed changes in membrane affinities due to cysteine substitution and fluorescein labeling. Membrane affinity is decreased 4−5-fold upon cysteine substitution for Phe^{35} or Tyr^{96} in the first or second Ca^{2+}-binding loop, respectively, indicating that these residues are especially important in membrane docking. Fluorescein labeling at position 98 in the third Ca^{2+}-binding loop increases the membrane affinity 4−5-fold, suggesting that this modification stabilizes the protein−membrane interface.

The proposed model for membrane docking, in which all three Ca^{2+}-binding loops directly contact the membrane surface, explains a number of previous findings obtained for

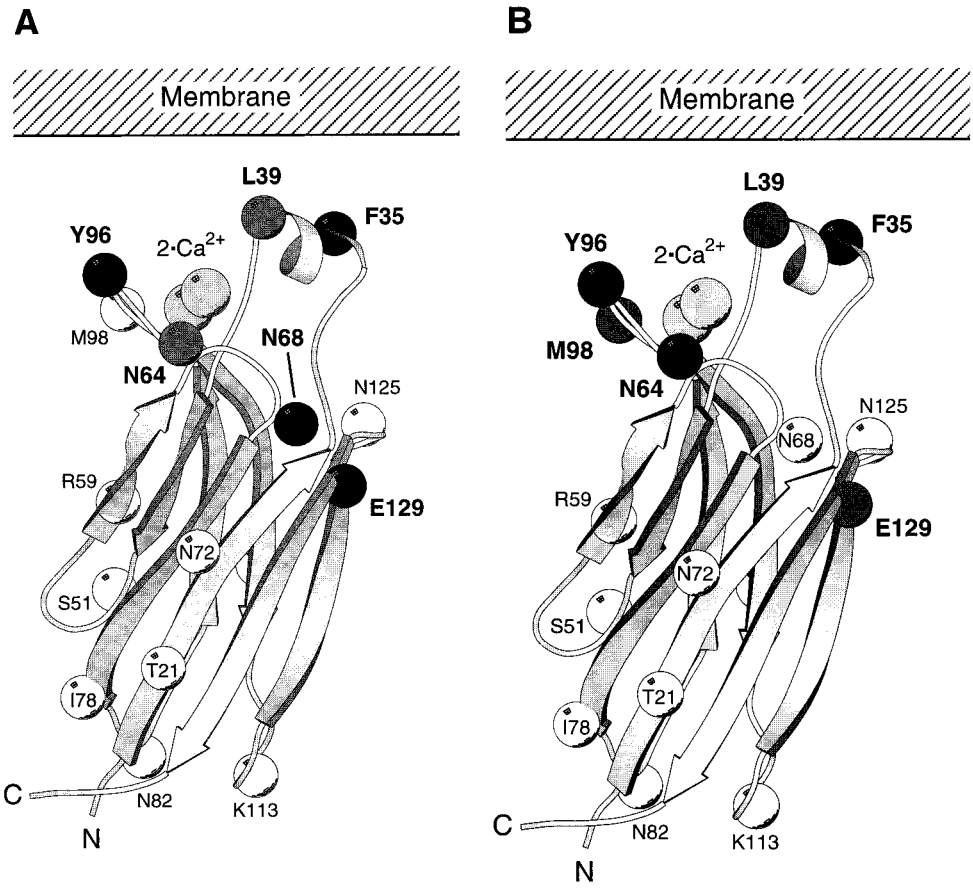

FIGURE 4: Mapping fluorescein-detected effects on the structure of the C2 domain. Ribbon diagram of the crystal structure of the $cPLA_2$ C2 domain (*9*), showing the two activating Ca^{2+} ions and the 16 positions of site-directed fluorescein labeling, the latter indicated as α-carbon spheres. Position T106 on the far surface is largely obscured and not numbered. (A) Ca^{2+}-triggered effects. Labeling positions where Ca^{2+} induces fluorescein emission increases are indicated in black; positions quenched by Ca^{2+} are dark gray; unperturbed positions are white. (B) Membrane-triggered effects. Positions where docking to PC membranes induces substantial fluorescein quenching are dark gray; the black positions exhibit both substantial quenching and protection from iodide collisions. For experimental details, see Figure 2, panels C and D. The modeled orientation is proposed to occur as the free domain docks to the membrane; subsequently, the membrane-docking loops likely undergo structural changes and certain hydrophobic side chains may be submerged in the hydrocarbon phase of the bilayer. This figure was drawn with MOLSCRIPT (*43*). The present results cannot specify the precise docking angle between the domain and membrane surface.

the C2 domains of $cPLA_2$ and other proteins. The two Ca^{2+} ions bound to the $cPLA_2$ C2 domain become occluded upon membrane docking, such that their on- and off-rates both slow by orders of magnitude (*16*). This observation is consistent with the developing picture in which the membrane surface forms a "lid" over the Ca^{2+}-binding cleft, perhaps allowing direct Ca^{2+} coordination by phospholipid headgroups. The model is further strengthened by the observation that backbone nuclei in each Ca^{2+}-binding loop undergo NMR chemical shift changes upon micelle docking, either due to direct lipid contacts or allosteric structural changes (*10*). Results obtained for other C2 domains suggest that at least one or two Ca^{2+}-binding loops are also involved in membrane docking (*22*−*25*). The present findings for the $cPLA_2$ C2 domain, which are the first to demonstrate burial at the membrane surface of probes on all three Ca^{2+}-binding loops, raise the possibility that all three loops make direct membrane contact in other C2 domains as well.

Finally, this model is consistent with the contrasting headgroup selectivities of different C2 domains. Sequence alignments show that the Ca^{2+}-binding loops of C2 domains from $cPLA_2$, synaptotagmin I (SytI), and protein kinase Cβ (PKCβ) all possess hydrophobic side chains that could favor membrane docking. The present model of $cPLA_2$ membrane docking, for example, orients several hydrophobic residues toward the membrane surface, including the residues Phe^{35}, Leu^{39}, Met^{98}, and Tyr^{96}, providing a structural basis for previous observations that hydrophobic interactions are involved in docking of this C2 domain to PC membranes (*14*, *15*, *39*). Such hydrophobic interactions, however, cannot explain the preference of the $cPLA_2$ C2 domain for the zwitterionic PC headgroup and the preference of SytI and PKCβ C2 domains for anionic PS headgroups. In this regard, comparison of the noncoordinating residues in the Ca^{2+}-binding loops of these domains reveals that the second and third Ca^{2+}-binding loops of SytI and PKCβ possess multiple basic charges that could favor anionic headgroups (*23*, *24*). The present findings emphasize that all three loops may contribute to selectivity: in $cPLA_2$, for example, the three Ca^{2+}-binding loops lack basic residues but possess noncoordinating acidic side chains that may explain the ability of this domain to reject anionic headgroups.

Finally, the surface-scanning approach utilized in the present study may be of general utility in delineating docking surfaces in protein−membrane and protein−protein interactions. An advantage of this approach is that the scanning

residue, cysteine, is often nonperturbing, especially when introduced at protein surfaces (*40*−*42*). Although covalent attachment of a bulky fluorescent probe will sometimes disrupt a docking interface, such findings are useful since they help localize the region involved in docking. Moreover, the present results demonstrate that the fluorescein quantum yield and protonation state are both sensitive indicators of local environmental changes and docking interactions. In short, site-directed fluorescein probes provide both functional and spectroscopic information that can be used to map out the region of a protein surface involved in intermolecular contacts.

ACKNOWLEDGMENT

The authors wish to acknowledge the expert assistance of Mark A. Wisner in the isolation of variant proteins.

REFERENCES

1. Brose, N., Hofmann, K., Hata, Y., and Südhof, T. C. (1995) *J. Biol. Chem. 270*, 25273.
2. Ponting, C. P., and Parker, P. J. (1996) *Protein Sci. 5*, 162.
3. Nalefski, E. A., and Falke, J. J. (1996) *Protein Sci. 5*, 2375.
4. Rizo, J., and Südhof, T. C. (1998) *J. Biol. Chem. 273*, 15879.
5. Sutton, R. B., Davletov, B. A., Berghuis, A. M., Südhof, T. C., and Sprang, S. R. (1995) *Cell 80*, 929.
6. Essen, L.-O., Perisic, O., Katan, M., and Williams, R. L. (1996) *Nature 380*, 595.
7. Grobler, J. A., Essen, L.-O., Williams, R. L., and Hurley, J. H. (1996) *Nat. Struct. Biol. 3*, 788.
8. Essen, L.-O., Perisic, O., Lynch, D. E., Katan, M., and Williams, R. L. (1997) *Biochemistry 36*, 2753.
9. Perisic, O., Fong, S., Lynch, D. E., Bycroft, M., and Williams, R. L. (1998) *J. Biol. Chem. 273*, 1596.
10. Xu, G.-Y., McDonagh, T., Yu, H.-A., Nalefski, E. A., Clark, J. D., and Cumming, D. A. (1998) *J. Mol. Biol. 280*, 485.
11. Clark, J. D., Schievella, A. R., Nalefski, E. A., and Lin, L.-L. (1995) *J. Lipid Mediat. Cell Signaling 12*, 83.
12. Leslie, C. C. (1997) *J. Biol. Chem. 272*, 16709.
13. Clark, J. D., Lin, L.-L., Kriz, R. W., Ramesha, C. S., Sultzman, L. A., Lin, A. Y., Milona, N., and Knopf, J. L. (1991) *Cell 65*, 1043.
14. Nalefski, E. A., Sultzman, L. A., Martin, D. M., Kriz, R. W., Towler, P. S., Knopf, J. L., and Clark, J. D. (1994) *J. Biol. Chem. 269*, 18239.
15. Nalefski, E. A., McDonagh, T., Somers, W., Seehra, J., Falke, J. J., and Clark, J. D. (1998) *J. Biol. Chem. 273*, 1365.
16. Nalefski, E. A., Slazas, M. M., and Falke, J. J. (1997) *Biochemistry 36*, 12011.
17. Ubach, J., Zhang, X., Shao, X., Südhof, T. C., and Rizo, J. (1998) *EMBO J. 17*, 3921.
18. Linse, S., and Forsén, S. (1995) *Adv. Second Messenger Phosphoprotein Res. 30*, 89.
19. Falke, J. J., Drake, S. K., Hazard, A. L., and Peersen, O. B. (1994) *Q. Rev. Biophys. 27*, 219.
20. Tanaka, T., Ames, J. B., Harvey, T. S., Stryer, L., and Ikura, M. (1995) *Nature 376*, 444.
21. Swairjo, M. A., Concha, N. O., Kaetzel, J. R., and Seaton, B. A. (1995) *Nat. Struct. Biol. 2*, 968.
22. Edwards, A. S., and Newton, A. C. (1997) *Biochemistry 36*, 15615.
23. Medkova, M., and Cho, W. (1998) *J. Biol. Chem. 273*, 17544.
24. Zhang, X., Rizo, J., and Südhof, T. C. (1998) *Biochemistry 37*, 12395.
25. Chapman, E. R., and Davis, A. F. (1998) *J. Biol. Chem. 273*, 13995.
26. Nalefski, E. A., Shaw, K. T. Y. S., and Rao, A. (1995) *J. Biol. Chem. 270*, 22351.
27. Hazard, A. L., Kohout, S. C., Stricker, N. L., Putkey, J. A., and Falke, J. J. (1998) *Protein Sci. 7*, 2451.
28. Lehrer, S. (1971) *Biochemistry 10*, 3254.
29. Lakowicz, J. R. (1983) *Principles of Fluorescence Spectroscopy*, Plenum Press, New York.
30. Lakowicz, J. R., Laczko, G., Gryczynski, I., Szmacinski, H., and Wiczk, W. (1989) *Ber. Bunsen-Ges. Phys. Chem. 93*, 316.
31. Haugland, R. P. (1996) *Handbook of Fluorescent Probes and Research Chemicals*, Molecular Probes, Eugene, OR.
32. Friedrich, S. and Wooley, P. (1988) *Eur. J. Biochem. 173*, 227.
33. Stanton, S. G., Kantor, A. B., Petrossian, A., and Owicki, J. C. (1984) *Biochim. Biophys. Acta 776*, 228.
34. Sjöback, R., Nygren, J. and Kubista, M. (1995) *Spectrochim. Acta A51*, L7.
35. de Kroon, A. I. P. M. (1994) *FEBS Lett. 342*, 230.
36. Thulborn, K. R., and Sawyer, W. H. (1978) *Biochim. Biophys. Acta 511*, 125.
37. Watt, R. M., and Voss, E. W. (1979) *J. Biol. Chem. 254*, 1684.
38. Shao, X., Davletov, B. A., Sutton, R. B., Südhof, T. C., and Rizo, J. (1996) *Science 273*, 248.
39. Davletov, B., Perisic, O., and Williams, R. L. (1998) *J. Biol. Chem. 273*, 19093.
40. Falke, J. J., and Koshland, D. E. (1987) *Science 25*, 7895.
41. Careaga, C. L., and Falke, J. J. (1992) *J. Mol. Biol. 226*, 1219.
42. Sahintoth, M., and Kaback, H. R. (1993) *Protein Sci. 2*, 1024.
43. Kraulis, P. J. (1991) *J. Appl. Crystallogr. 24*, 946.
44. Grobler, J. A., and Hurley, J. H. (1998) *Biochemistry 37*, 5020.

BI982372E